

# STM topography and manipulation of single Au atoms on Si(100)

F. Chiaravallotti, D. Riedel, and G. Dujardin

*Laboratoire de Photophysique Moléculaire, Université Paris Sud, CNRS UPR 3361, Bâtiment 210, 91405 Orsay, France*

H. P. Pinto and A. S. Foster

*Department of Applied Physics, Helsinki University of Technology, P.O. Box 1100, FIN-02015 TKK, Finland**and Department of Physics, Tampere University of Technology, P.O. Box 692, FIN-33101, Finland*

(Received 2 April 2009; published 30 June 2009)

The low-temperature (12 K) adsorption of single Au atoms on Si(100) is studied by scanning tunneling microscopy (STM). Comparison between experimental and calculated STM topographies as well as density-functional-theory calculations of the adsorption energies enable us to identify two adsorption configurations of Au atoms between Si-dimer rows (BDRs) and on top of Si-dimer rows (TDRs). In both adsorption configurations, the Au atoms are covalently bound to two Si atoms through a partial electron transfer from Si to Au. STM manipulation confirms that the TDR adsorption configuration is metastable, whereas the BDR one is the most stable configuration.

DOI: [10.1103/PhysRevB.79.245431](https://doi.org/10.1103/PhysRevB.79.245431)

PACS number(s): 68.37.Ef, 68.43.Fg, 68.47.Fg

## I. INTRODUCTION

Adsorption of gold on silicon surfaces is of utmost interest in a number of applications. For example, gold nanoislands and nanoparticles are extensively used as metal catalysts for the synthesis of one-dimensional nanostructures such as silicon nanowires<sup>1</sup> and carbon nanotubes.<sup>2</sup> Gold covered silicon surfaces also show interesting mesoscopic structures<sup>3–8</sup> as well as optical properties.<sup>9</sup> Furthermore, the presence of a gold monolayer on silicon has been shown to radically influence the growth process of silicon oxide,<sup>10</sup> iron,<sup>11,12</sup> and other more complex materials.<sup>13–15</sup>

In recent years, thin films of Au on Si(100) surface have been investigated at different coverages with different spectroscopic techniques but the description of such Au films is still extremely controversial.<sup>16–21</sup> The early stages of growth at room temperature have been studied with a scanning tunneling microscope (STM) and some models of growth have been proposed,<sup>22–24</sup> but the positions of individual Au atoms on the Si(100) surface are still unknown.<sup>25,26</sup> A study of the early stage of growth is needed to understand the process of creation of the Au/Si interface. A theoretical study has been carried out,<sup>25</sup> suggesting which adsorption sites within the Si unit cell are the most favorable for an Au atom. However, the usual  $2 \times 1$  reconstruction of the real Si(100) surface was not considered.<sup>27</sup> Furthermore, recent calculations suggest that the growth process is different if the substrate temperature is below room temperature.<sup>28</sup> Similar temperature dependent adsorption configurations have been observed for the adsorption of biphenyl molecules on Si(100).<sup>29</sup>

In this paper, we investigate experimentally and theoretically the initial stage of Au adsorption on Si(100) at low temperature (12 K). Comparison between experimental and calculated STM topographies as well as density-functional-theory (DFT) calculations of the Au adsorption-energy pathways enable us to unambiguously identify the various adsorption configurations of single Au atoms on Si(100).

## II. EXPERIMENTAL AND THEORETICAL METHODS

Experiments are performed in an ultrahigh-vacuum (UHV) apparatus divided into a preparation chamber and a

low-temperature STM (LT-STM) chamber. The clean (100) surface of a *n*-type As-doped silicon sample (resistivity 5 m $\Omega$  cm) is prepared as explained elsewhere.<sup>27</sup> During the Au evaporation, the Si substrate is kept at a temperature of about 12 K using a liquid-He cooling system. Gold is evaporated by heating a tungsten filament covered by gold wires and located a few centimeters in front of the Si(100) substrate. The current flowing through the filament during the evaporation is 4 A. To obtain a coverage of 3–4 % (measured as the number of Au atoms per Si dimer) required an evaporation time of 4 min. After the Au deposition, the sample is transferred in UHV into the LT-STM chamber where the sample and the microscope are held at 9 K.

DFT calculations are performed using the plane-wave basis Vienna *ab initio* simulation package (VASP),<sup>30,31</sup> implementing the generalized gradient approximation by Perdew, Burke, and Ernzerhof (PBE) (Ref. 32) and the projector-augmented-wave potentials (for Au, the 5*d* and 6*s* valence states are considered). Using a cutoff kinetic energy of 380 eV and a  $\Gamma$  centered *k*-point mesh with a separation of 0.02  $\text{\AA}^{-1}$ , we converge the energy to values  $<1$  meV/f.u. (f.u.=formula unit Si fcc). The structures are fully relaxed until all the forces are below 0.01 eV/ $\text{\AA}$ . We first compute the PBE optimal structure for bulk Si fcc with a predicted lattice constant of 5.47  $\text{\AA}$ . Next, we compute the properties of a single Au atom deposited on a Si(100) surface using a  $6 \times 6$  Si(100) supercell. This slab is five layers thick and the Si atoms of the bottom layer are passivated with hydrogen. This Si-H layer is kept fixed during ionic relaxation. The nudged elastic band method<sup>33</sup> is used for identifying the Au reaction-energy path. The constant current STM images are simulated using the Tersoff-Hamman approximation implemented in the BSKAN code.<sup>34</sup> This code uses the real-space single-electron wave functions of the slab computed previously with VASP.

## III. RESULTS AND DISCUSSION

### A. Experimental STM topographies of Au atoms on Si(100)

A typical STM topography of the Si(100) surface after Au atom deposition is shown in Fig. 1. The bright vertical lines

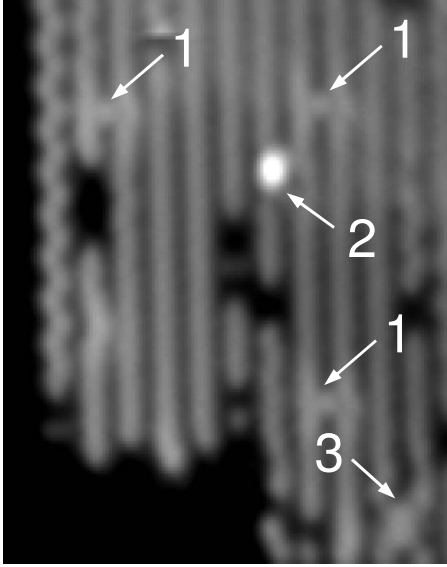


FIG. 1.  $93 \times 117 \text{ \AA}^2$  STM topography of the silicon surface after adsorption of Au atoms (9 K). Arrows (1) or (3) indicate the position of BDR Au-atoms configurations while arrow (2) indicates the TDR Au atom.

are the silicon-dimer rows of the  $(2 \times 1)$  reconstructed Si(100) surface. Several new features appear in the STM topography after Au evaporation. They are visible in Fig. 1 as (i) bright features between silicon-dimer rows (BDRs) (labeled 1 and 3), (ii) bright features located on top of the dimer rows (TDRs) (labeled 2), and (iii) dark features along the silicon-dimer rows. Before Au evaporation, dark features are present on the surface in low quantities (1–2 % of the total number of silicon dimers) due to either missing silicon dimers or the adsorption of water molecules.<sup>35</sup> After Au evaporation, the number of dark features increases, possibly due to the adsorption of water molecules desorbed from the gold evaporator or to the adsorption of Au atoms themselves. In the following, we will discuss only the bright features (labeled as 1, 2, and 3) which can be unambiguously assigned to the adsorption of Au atoms.

More detailed STM topographies of these Au-related structures are shown in Figs. 2 and 3. The BDR structure is the most frequently observed with a density of  $2.5 \pm 0.2 \%$  Au atoms/Si dimer. This structure is observed alone (label 1 in Fig. 1) or in pairs (label 2 in Fig. 1). A single BDR structure is shown in Figs. 2(a) and 2(b) as imaged with the LT-STM at different surface voltages. The topography in Fig. 2(a) is taken at a surface voltage  $V_s = -2.0$  V. The Si-dimer rows are visible as vertical bright lines in which individual Si dimers can be seen. The bright spot is assigned to a single Au atom adsorbed between two Si-dimer rows. Along the vertical direction the Au atom is aligned with the Si dimers. In Fig. 2(b), the same structure is imaged at  $V_s = +0.75$  V. At this surface voltage, the Au atom is imaged as a protrusion between the dimer rows while the Si-dimer rows on either side show a zigzag structure due to the buckling of Si dimers.<sup>27</sup> In Fig. 2(b), the Si dimer on the left side of the Au atom appears brighter than the Si dimer located to the right. This asymmetry is due to a difference in the buckling between the two Si dimers.

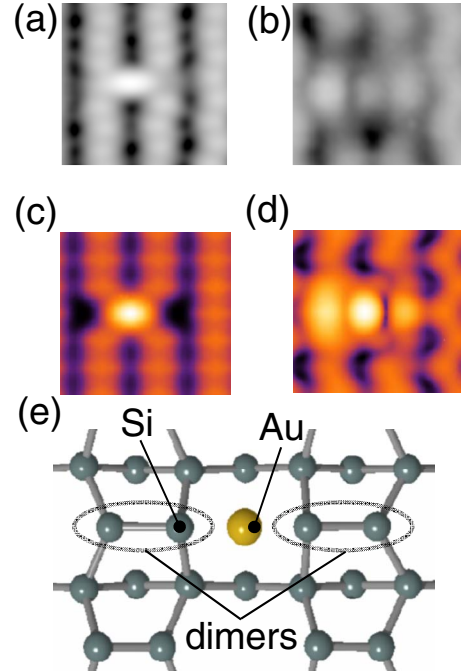


FIG. 2. (Color online) (a) and (b) are  $19.2 \times 19.2 \text{ \AA}^2$  STM topographies ( $I = 70$  pA) of an Au atom in the BDR configuration at  $V_s = -2$  V and  $V_s = +0.75$  V, respectively. (c) and (d) are the  $19.2 \times 17 \text{ \AA}^2$  calculated STM topographies of (a) and (b). (e) is a ball-and-stick representation of the BDR configuration used for the calculation of (c) and (d).

The less frequently observed TDR structure (label 2 in Fig. 1) is shown in more detail in Figs. 3(a) and 3(b) for  $V_s = -2$  V and  $V_s = +2$  V, respectively. The density of this TDR structure ( $0.3 \pm 0.1 \%$  Au atoms/Si dimer) is ten times smaller than the BDR structure. In Fig. 3, the bright protrusion assigned to the Au atom is located on the Si-dimer row. Here, the dimer row is imaged as a bright line at a negative-bias voltage ( $-2$  V) and as a dark line at positive bias ( $+2$  V).

### B. Calculated adsorption configurations and STM topographies of Au atoms on Si(100)

The computed adsorption configurations of Au atoms on Si(100) are shown in Fig. 4. After full relaxation, the PBE results (Table I) indicate a global minimum energy ( $-3.24$  eV) when the Au atom is adsorbed between two Si-dimer rows (BDR configuration, Fig. 4). We also find two metastable adsorption configurations when the Au atom is adsorbed on top of a Si-dimer row [TDR(1) and TDR(2), Figs. 4(b) and 4(c), respectively]. In all these three configurations, the Au atom is covalently bonded to two Si atoms through Si(*p*)-Au(*d*) hybridization. This is in agreement with recent studies of adsorption of Au on Si(111)- $(7 \times 7)$ ,<sup>36</sup> where the authors have shown that Au adsorbs at high coordination sites, thus saturating the maximum number of Si dangling bonds. Since the Au atom is more electronegative than the Si atom, the covalent bonding between Au and Si has some ionic character, resulting in charge transfer from Si to Au. This is shown in Fig. 5 where we plot the charge-

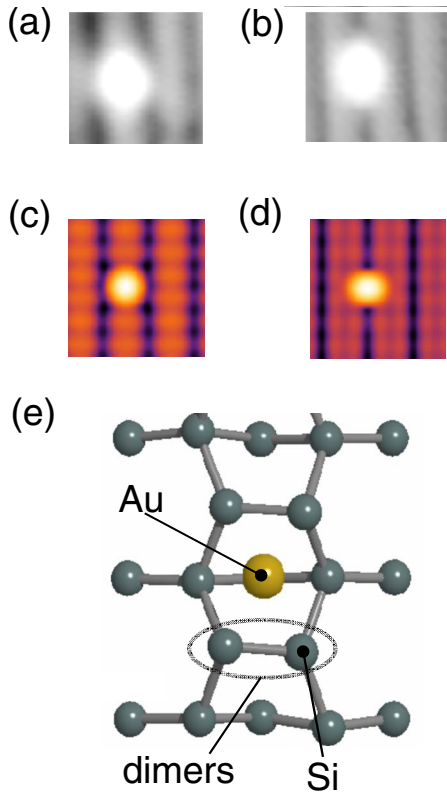


FIG. 3. (Color online) (a) and (b) are  $19.2 \times 19.2 \text{ \AA}^2$  STM topographies ( $I=70 \text{ pA}$ ) of an Au atom in the TDR(2) configuration at  $V_s=-2 \text{ V}$  and  $V_s=+2 \text{ V}$ , respectively. (c) and (d) are the  $19.2 \times 17 \text{ \AA}^2$  calculated STM topographies of (a) and (b). (e) is a ball-and-stick representation of the TDR(2) configuration used for the calculation of (c) and (d).

density contour for the BDR and TDR(2) configurations. The charge-density contours are obtained by integrating the density of charge over all the valence electrons of  $\text{Au}(5d^{10}6s^1)$  and  $\text{Si}(3s^23p^2)$ .

From results in Table I, the TDR(1) configuration is found to be slightly more stable than the TDR(2) one, although the difference in their adsorption energies is less than 0.1 eV. However, our experimental STM topographies rarely show the asymmetric TDR configuration (less than 1% of the total number of adsorbed atoms). In most cases, the Au atom is observed adsorbed symmetrically on top of a Si dimer as in the TDR(2) configuration (see Fig. 3). It is difficult to assign the rare asymmetric STM topographies that have been observed to the TDR(1) configuration since the observed asymmetry might be due to nearby defects on the surface.

The calculated STM topographies of the BDR and TDR(2) configurations are compared with the experimental

TABLE I. PBE minimum-energy values of the various adsorbed Au-atom configurations on the silicon surface with the corresponding Si-Au-Si angles.

	BDR	TDR(1)	TDR(2)
Binding energies (eV)	-3.24	-3.03	-2.94
Si-Au-Si angle (deg)	131	97.5	117.7

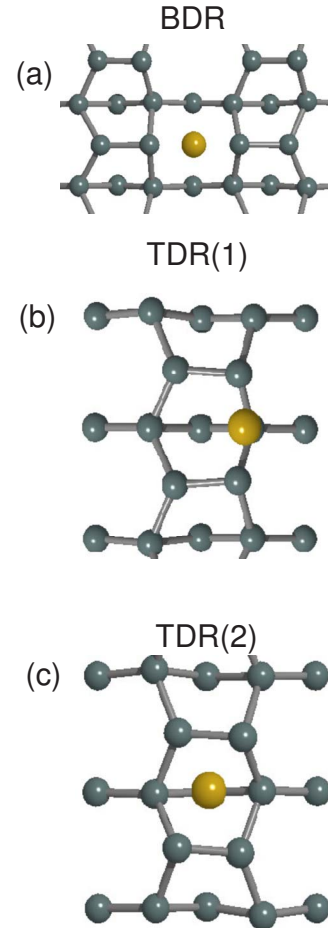


FIG. 4. (Color online) [(a)–(c)] Ball-and-stick representations of the BDR, TDR(1), and TDR(2) configurations, respectively.

STM topographies in Figs. 2(c)–2(e) and 3(c)–3(e), respectively. For both negative (occupied states) and positive (unoccupied) surface voltages, there is a good agreement between the experimental and calculated STM topographies. The asymmetry of the experimental STM topography at  $V_s=0.75 \text{ V}$  [Fig. 2(b)], related to the buckling of the neighboring Si dimers (see part III.1), is well reproduced in the calculated topography [see Fig. 2(d)]. We note that the changes in brightness of the Si-dimer rows when varying the surface voltage are also well reproduced by calculations in Figs. 2 and 3.

### C. Single Au-atom STM manipulation

The observed BDR and TDR(2) adsorption configurations are stable; no changes were seen even after repeated STM topographies under normal scanning conditions (surface voltage between  $-2$  and  $+2 \text{ V}$ , tunnel current around  $70 \text{ pA}$ ). In order to test further their stability, we attempted to change the adsorption configuration by STM manipulation. After recording the STM topography of an Au atom in the BDR or TDR(2) configuration, the STM tip is placed on top of the center of the Au atom, the feedback loop is switched off, the STM tip is approached toward the surface by  $0.1 \text{ nm}$  with respect to the imaging conditions ( $V_s=-2 \text{ V}$  and  $I=70 \text{ pA}$ )

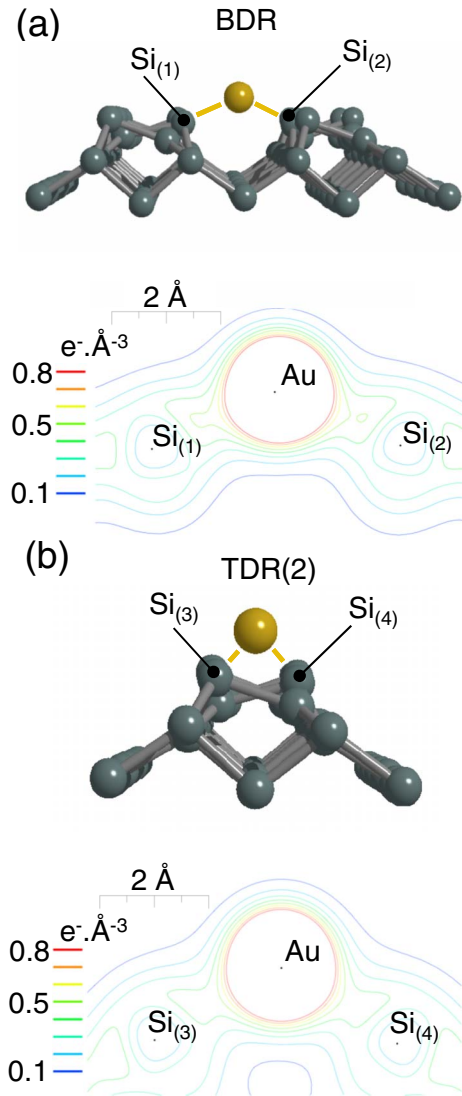


FIG. 5. (Color online) (a) and (b) are charge-density contour of the BDR and TDR(2) configurations, respectively.

and a positive surface voltage  $V_S=3$  V is applied for 1 s. During this voltage pulse, the tunnel current is recorded as a function of time as shown in Fig. 6(c). The abrupt change in tunnel current indicates that the Au atom has moved or has changed its adsorption configuration. Afterwards, a new STM topography is recorded to check the position and the configuration of the Au atom.

The STM manipulation of a Au atom initially in the TDR(2) configuration is shown in Fig. 6(a). After manipulation, the Au atom is found in the BDR configuration [Fig. 6(b)]. STM manipulation of an Au atom initially in the BDR configuration always results (30 attempts) in the diffusion of the Au atom across the surface to another BDR site; there is no conversion to the other adsorption configuration. The diffusion is over a distance of one or two intersilicon dimers. The reason why the transformation of the BDR configuration into the TDR(2) one is not observed cannot be understood only from the stability of these two configurations since the binding energies of these two configurations are very similar. This is most probably related to the mechanisms of

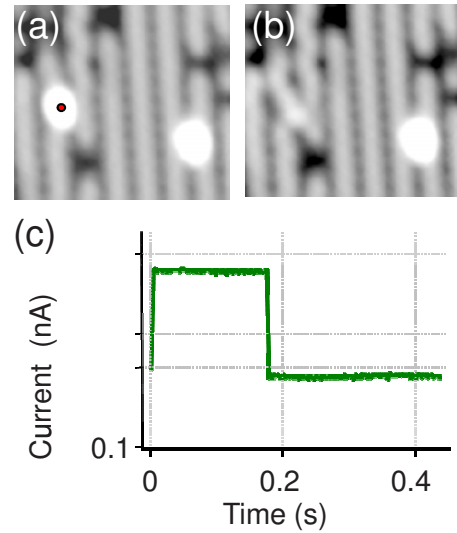


FIG. 6. (Color online) (a) and (b) are  $57.8 \times 52.8 \text{ \AA}^2$  STM topographies ( $V_S=-2$  V and  $I=70$  pA) of Au atoms adsorbed on the Si(100)- $2 \times 1$  surface before and after a manipulation, respectively. (c) is the recorded current trace during the manipulation applied on the left Au atom in (a) (shown by the dot).

the electronic excitation induced with the STM tip. Indeed, it is known that molecular reactions having similar activation energies can be very selectively activated by electronic excitation with the STM tip.<sup>37</sup>

#### IV. CONCLUSION

We have investigated the adsorption of Au atoms on the Si(100) surface at 12 K using a low-temperature STM. DFT calculations have been performed to calculate the adsorption energies of various adsorption configurations and the energy barriers between configurations. Experimental and calculated STM topographies have been compared to identify the observed adsorption configurations.

The most frequently observed adsorption configuration is the BDR configuration where the Au atom lies between two Si-dimer rows and is bonded to two silicon atoms. This configuration is the most stable one, and it has the minimum computed energy. Under STM manipulation, Au atoms in BDR configuration are found to diffuse to other equivalent BDR sites. The TDR(2) configuration is observed with a much reduced frequency. It consists of a Au atom centered on top of a Si dimer and bonded to the two Si atoms of the dimer. This configuration is calculated to be metastable and can be transformed into the BDR configuration by STM manipulation. In both BDR and TDR(2) configurations, the Au atom is covalently bonded to two Si atoms through Si(*p*)-Au(*d*) hybridization. However, the covalent bonding between Au and Si has some ionic character due to electron transfer from Si to Au.

These results demonstrate the feasibility of atomic-scale studies of adsorption of gold on Si(100) surfaces. Further experiments would be necessary to understand the adsorption of gold at other temperatures. In particular, at room temperature or higher temperatures, one might envisage more com-

plex adsorption configurations involving subsurface adsorption. This work also opens interesting perspectives to investigate higher coverages of gold on Si(100) and the subsequent formation of nanostructures (islands, wires).

## ACKNOWLEDGMENTS

This work was supported by the European Integrated Project PicoInside (Contract No. FPG-015847).

- 
- <sup>1</sup>J. B. Hannon, S. Kodambaka, F. M. Ross, and R. M. Tromp, *Nature (London)* **440**, 69 (2006).
- <sup>2</sup>S. Bhaviripudi, E. Mile, S. A. Steiner III, A. T. Zare, M. S. Dresselhaus, A. M. Belcher, and J. Kong, *J. Am. Chem. Soc.* **129**, 1516 (2007).
- <sup>3</sup>W. H. Choi, P. G. Kang, K. D. Ryang, and H. W. Yeom, *Phys. Rev. Lett.* **100**, 126801 (2008).
- <sup>4</sup>F. Heringdorf, *J. Phys.: Condens. Matter* **18**, S1 (2006).
- <sup>5</sup>F.-J. Meyer zu Heringdorf, K. L. Roos, C. Wiethoff, M. Horn-von Hoegen, and K. R. Roos, *Surf. Sci.* **602**, 1852 (2008).
- <sup>6</sup>M. Horn-von Hoegen, F.-J. Meyer zu Heringdorf, R. Hild, P. Zahl, Th. Schmidt, and E. Bauer, *Surf. Sci.* **435**, 475 (1999).
- <sup>7</sup>J. H. He, W. W. Wu, Y. L. Chueh, C. L. Hsin, L. J. Chen, and L. J. Chou, *Appl. Phys. Lett.* **87**, 223102 (2005).
- <sup>8</sup>M. M. Giangregorio, M. Losurdo, A. Sacchetti, P. Capezzuto, and G. Bruno, *J. Lumin.* **121**, 322 (2006).
- <sup>9</sup>H. Minoda and N. Yamamoto, *J. Phys. Soc. Jpn.* **74**, 1914 (2005).
- <sup>10</sup>G. Leclerc, L. Paquin, and F. Baratay, *J. Mater. Res.* **7**, 2458 (1992).
- <sup>11</sup>S. -Y. Wei, J.-G. Wang, L. Ma, C.-X. Xia, and Y.-L. Yan, *Chin. Phys.* **13**, 932 (2004).
- <sup>12</sup>F. Zavaliche, W. Wulfhekkel, M. Przybylski, S. Bodea, J. Grabowski, and J. Kirschner, *J. Phys. D* **36**, 779 (2003).
- <sup>13</sup>G. Ramanath, H. Z. Xiao, S. L. Lai, L. H. Allen, and T. L. Alford, *J. Appl. Phys.* **79**, 3094 (1996).
- <sup>14</sup>S. L. Cheng and H. Y. Chen, *Thin Solid Films* **516**, 8797 (2008).
- <sup>15</sup>H. Minoda, Y. Tanishiro, N. Yamamoto, and K. Yagi, *Surf. Sci.* **333**, 913 (1995).
- <sup>16</sup>W. C. A. N. Ceelen, B. Moest, M. de Ridder, L. J. van IJzendoorn, A. W. Denier van der Gon, and H. H. Brongersma, *Appl. Surf. Sci.* **134**, 87 (1998).
- <sup>17</sup>G. Yang, J. H. Kim, S. Yang, and A. H. Weiss, *Surf. Sci.* **367**, 45 (1996).
- <sup>18</sup>K. Hricovini, J. E. Bonnet, B. Carrière, J. P. Deville, M. Hanbücken, and G. L. Lay, *Surf. Sci.* **211**, 360 (1989).
- <sup>19</sup>Z. H. Lu, T. K. Sham, K. Griffiths, and P. R. Norton, *Solid State Commun.* **76**, 113 (1990).
- <sup>20</sup>E. Landree, D. Grozea, C. Collazo-Davila, and L. D. Marks, *Phys. Rev. B* **55**, 7910 (1997).
- <sup>21</sup>M. Kageshima, Y. Torii, Y. Tano, O. Takeuchi, and A. Kawazu, *Surf. Sci.* **472**, 51 (2001).
- <sup>22</sup>Y. Akira, T. Yasumasa and Y. Katsumichi, *Surf. Sci.* **264**, 55 (1992).
- <sup>23</sup>K. S. Kim *et al.*, *Nucl. Instrum. Methods Phys. Res. B* **117**, 289 (1996).
- <sup>24</sup>K. S. Kim, Y. W. Kim, N. G. Park, W. S. Cho, Y. C. Park, C. N. Whang, S. S. Kim, and D. S. Choi, *J. Korean Phys. Soc.* **31**, 140 (1997).
- <sup>25</sup>S.-Y. Wei, J. G. Wang, and L. Ma, *Chin. Phys.* **13**, 85 (2004).
- <sup>26</sup>W. W. Ju, T. W. Li, J. H. You, Z. X. Tang, X. Y. Gong, H. Wang, Z. Q. Zhen, and Q. G. Zhang, *Key Eng. Mater.* **368**, 1699 (2008).
- <sup>27</sup>D. Riedel, M. Lastapis, M. Martin and G. Dujardin, *Phys. Rev. B* **69**, 121301(R) (2004).
- <sup>28</sup>W. W. Ju and T. W. Li, *Key Eng. Mater.* **336**, 2521 (2007).
- <sup>29</sup>M. Martin, M. Lastapis, D. Riedel, G. Dujardin, M. Mamatkulov, L. Stauffer, and P. Sonnet, *Phys. Rev. Lett.* **97**, 216103 (2006).
- <sup>30</sup>G. Kresse and J. Furthmüller, *Phys. Rev. B* **54**, 11169 (1996).
- <sup>31</sup>G. Kresse and J. Furthmüller, *Comput. Mater. Sci.* **6**, 15 (1996).
- <sup>32</sup>J. P. Perdew, K. Burke, and M. Ernzerhof, *Phys. Rev. Lett.* **77**, 3865 (1996).
- <sup>33</sup>G. Henkelman and H. Jonsson, *J. Chem. Phys.* **113**, 9978 (2000).
- <sup>34</sup>K. Palotas and W. A. Hofer, *J. Phys.: Condens. Matter* **17**, 2705 (2005).
- <sup>35</sup>S.-Y. Yu, H. Kim, and J.-Y. Koo, *Phys. Rev. Lett.* **100**, 036107 (2008).
- <sup>36</sup>C. Zhang, G. Chen, K. Wang, H. Yang, T. Su, C. T. Chan, M. M. T. Loy, and X. Xiao, *Phys. Rev. Lett.* **94**, 176104 (2005).
- <sup>37</sup>D. Riedel, M.-L. Bocquet, H. Lesnard, M. Lastapis, N. Lorente, P. Sonnet, and G. Dujardin, *J. Am. Chem. Soc.* **131**, 7344 (2009).